Mutagenic Compounds as Broad Spectrum Antivirals

By
Collin S. Hill

Senior Honors Thesis
Department of Biology
University of North Carolina at Chapel Hill
4-28-2020

Approved:

_____

Dr. Ronald Swanstrom, Thesis Advisor

Dr. Mark Peifer, Reader

Dr. Chris Willett, Reader

Mutagenic Compounds as Broad Spectrum Antivirals

Collin S. Hill[1], Timothy P. Sheahan[1],Derek Carbaugh[1], Durbadal Ojha[2], Sabrina Sizemore[1], Amy C. Sims[1], Ralph Baric[1], Helen Lazear[1], Karin E. Peterson[2], Ronald Swanstrom[1], Shuntai Zhou[1]

1. University of North Carolina at Chapel Hill
2. Rocky Mountain Laboratories, NIAID/NIH

Abstract

Most RNA viruses utilize RNA-dependent RNA polymerases for viral genome replication and synthesis of mRNAs, making them prime targets for mutagenic compounds to be utilized as broad-spectrum antivirals. Primer ID with next-generation sequencing (NGS) allows for accurate and deep characterization of viral populations, which provides for the ideal tool for screening mutagenic compounds and their effects on RNA viruses. In this study, we used this approach to study three potential mutagenic compounds (N4-beta-hydrocytidine, Favipiravir, and Ribavirin) on a panel of RNA viruses, including MERS coronavirus (MERS-CoV), Zika virus (ZIKV), and La Crosse virus (LACV). We hypothesize that these compounds exhibit antiviral effects by inducing lethal mutations in the viral genomes. We used a cell culture model where we grew the viruses in cell culture in the presence and absence of drugs, determined viral titers using plaque assays, and sequenced viruses at different time points to compare sequence differences by using primer ID and NGS. Using this data from the in vitro experiments, we developed a model to predict the percentage of defective viral genomes after treatment with mutagenic compounds. We also used an in vivo mice-MERS coronavirus model to study the antiviral effects and short-term toxicity of NHC. To study the long term toxicity of all three compounds, we used an 8E5 cell model, harboring a single HIV provirus per cell, to monitor the effects of these compounds on DNA dependent RNA polymerase (transcription) and DNA polymerase (DNA replication). The viral titers in the cell culture model showed that 10 μM of NHC had significant inhibition of MERS-CoV and LACV and moderate inhibition of ZIKV, which correlated strongly with an increase of cytosine (C) to uridine (U) transversion mutations, suggesting its mechanism for its antiviral activity is lethal mutagenesis. Both Favipiravir and Ribavirin exhibited no antiviral effects on MERS-CoV or ZIKV but had some antiviral effects on LACV. The In vivo mouse model showed that NHC had great inhibition in MERS-CoV with no significant observed mutations in the mice mRNA. The 8E5 cell model showed that neither Ribavirin or Favipiravir increased the mutation rate, but found that NHC caused an increase in the C to U mutations, suggesting there may be some long term effects of the drug. With the broad-spectrum antiviral effects of these compounds, they could potentially be able to be used to treat a wide variety of viral infections in humans, including newly emerged viruses that lack other forms of treatment.

Introduction

RNA viruses are the most common class of emerging infectious diseases, with up to 44% of all emerging infectious diseases being etiologically derived from RNA viruses (1,2). Many recent infectious disease outbreaks have been caused by emerging RNA viruses, including Zika virus, Dengue virus, H1N1 influenza virus, MERS coronavirus, and the most recently emerged, SARS coronavirus 2, the virus behind the COVID-19 outbreak (2,3). These RNA-viral emergent diseases pose a significant threat to public health, as the treatment of such diseases are limited due to the low number of approved antiviral drugs (4,5) and the prevention of such diseases requires the availability of vaccines, which can take years to develop (6) and are not always effective in preventing infection (4). In order to rapidly respond to RNA-viral disease outbreaks before they become global pandemics, there is a need for the identification of novel antiviral drug targets and for the development of broad-spectrum antivirals (4).

All RNA viruses (besides retroviruses) rely on RNA-Dependent RNA polymerases (RDRP) for viral genome replication and transcription (7). These viral RNA polymerases have notoriously low fidelity, typically due to the lack of proofreading activity, which leads to the characteristically high mutation rate of RNA viruses (7). When controlled for genome size, the average RNA virus mutation rate is about one base change per RNA genome replication cycle while the average DNA-based organism has a mutation rate that is much lower at 10^{-3} base change per DNA genome replication cycle (8,9).

These high mutation rates produce large amounts of genetic mutants and cause RNA virus populations to exhibit extreme genetic variation (8,9). With such high genetic variation, fast reproductive cycles, and high mutation rates, RNA virus populations can readily and quickly adapt to rapidly changing environments (5,9,10). This adaptive ability and high amounts of genetic diversity make it difficult to develop effective treatments, like targeted antivirals and vaccines, because viral populations can adapt relatively quickly and become resistant to the treatments (5,9,10).

While the high mutation rate of RNA viruses allows for significant adaptive advantage, the vast majority of these mutations are deleterious (11). This causes the viral populations to live close to their error threshold, where any additional deleterious mutations can lead to a significant decrease in mean fitness of the viral population(11,12). This characteristic of RNA viral populations has led to the testing of mutagenic compounds that would induce lethal mutagenesis, where the viral

populations would be pushed to extinction due to the accumulation of deleterious mutations by increasing the mutation rate of the virus past its error threshold (11,12). These mutagenic compounds can potentially be used as broad-spectrum antivirals in a clinical setting. Mutagenic compounds that would only affect the synthesis of new genomes and mRNA through the RNA-dependent RNA polymerase are particularly appealing for clinical application due to the fact that there is no analogous cellular process in eukaryotic cells (7). This means that the compound would mutate RNA viral genomes but would not likely cause changes to the DNA genome of the host. Another appealing aspect of lethal mutagenesis is that there is limited potential for developing resistant strains of virus due to the inherent nature of the viral RNA polymerases(5,9,13).

However, screening for new potential mutagenic compounds can be challenging because of the extreme genetic variability of the viral population and the presence of many rare mutants (14). Primer ID (PID) deep sequencing serves as an ideal method for screening mutagenic compounds as it rectifies some of the limitations of other sequencing methods, due to its ability to provide deep coverage while maintaining high accuracy with an error rate of 1 in 10,000 nucleotides (15,16). This is important to validate the detection of rare mutants and to verify the types of mutations caused by mutagenic compounds (14,15,16). PID deep sequencing utilizes primers with an embedded degenerate block of nucleotides to create a random library of sequences within the primer population (15,16,17). As the primers are used during the cDNA synthesis from the RNA, each cDNA complement has a unique sequence that can be used for identification (15,16). These identification sequences will remain attached to the original sequence even after subsequent PCR amplification (15,16). This approach corrects for both PCR resampling and recombination and allows for the creation of a template consensus sequence (TCS) by aligning all sequences with the same primer ID, greatly reducing the error rate caused by PCR and high throughput sequencing (15,16,17).

Using this PID sequencing method, we compare three potential broad spectrum antiviral compounds, β-D-N4-hydroxycytidine (NHC), ribavirin, and favipiravir, on a panel of viruses grown in cell culture, including MERS-CoV, Zika Virus, and La Crosse Virus. Previous research has had mixed results in determining the mechanism of action for each of these compounds (13,18,19,20,21,22,23), however we show that NHC across all three viruses, as well as ribavirin and favipiravir on La Crosse virus, acts through lethal mutagenesis for their antiviral effects. We also compare the three antiviral compounds on an 8E5 cell culture cytotoxicity assay, where we find that NHC increases the transcriptional error rate and may cause DNA replication errors.

Materials and Methods

Compounds

Ribavirin (Sigma Aldrich) and Favipiravir (AdooQ Bioscience) were obtained as solids to be mixed in DMSO. For the cell culture experiments, the β-D-N4-hydroxycytidine (NHC) was obtained through the NIH AIDS Reagent Program, Division of AIDS, NIAID, NIH, as a solid to be mixed in DMSO. The prodrug version of NHC, EIDD-2801, which was used in the in vivo experiments, was supplied by Emory University Institute for Drug Discovery (EIDD), as a solid to be mixed immediately prior to use. The solubilized compound needed each day was prepared in a vehicle containing 10% PEG400, 2.5% Cremophor RH40 in water (10/2.5/87.5%, all v/v).

Viral Strains

The viruses used for the cell culture experiments were MERS-CoV expression nanoluciferase (MERS-nLUC, TPS029, 16,000pfu/µl), Zika virus strain H/PF/2013, and La Crosse virus strain Human/78. The virus stock utilized for MERS-CoV in vivo experiment was derived from a plaque purified isolate of the mouse adapted MERS-CoV p35C4 strain.

MERS-CoV Drug Panel Cell Culture Experiment (Timothy Sheahan)

Vero ATCC CCL-81 cells were plated in a 12-well plate at $2.5x10^5$ cells/well with DMEM medium containing 5% FBS and were then infected with MERS-CoV nLUC at an MOI of 0.5. The infected vero cells were then incubated at 37˚C for 12hr. A panel of compounds were diluted to concentrations of 0.1 µM, 1.0 µM, and 10 µM for NHC and favipiravir from 10 mM stocks and 1.0 µM, 10 µM and 100 µM for ribavirin from a 100 mM stock. After 12hr post infection, the compounds were added to each of the wells, with two replicates for each of the compound concentrations, and two additional wells had DMSO added for vehicle controls. After 36hr post infection, the viral RNA was extracted using QIAamp viral RNA mini kit (Qiagen), which was then sent to our lab for primer ID library preparation. Then, using the protocol used in Sheahan *et al* 2020, the virus replication was quantified on a Spectramax (Molecular Devices) via nanoluciferase assay (NanoGlo Promega).

Zika Virus Drug Panel Cell Culture Experiment (Derek Carbaugh)

Vero ATCC CCL-81 cells were plated in a 12-well plate with DMEM medium containing 5% FBS and were infected with ZKV strain H/PF/2013 at an MOI of 0.5. The vero infected cells were then incubated at 37˚C for 24hr. A panel of compounds were diluted to concentrations of 0.1 µM, 1.0 µM, and 10 µM for NHC and favipiravir from 10 mM stocks and 1.0 µM, 10 µM and 100 µM for ribavirin from a 100 mM stock. After 24hr

post infection, the compounds were added to each of the wells, with two replicates for each of the compound concentrations, and two additional wells had DMSO added for vehicle controls. After 60hr post infection, the viral RNA was extracted using QIAamp viral RNA mini kit, which was then sent to our lab for primer ID library preparation. After 60hr post infection, a focus forming forming assay was used to determine infectivity. For this assay, the cell culture samples were serially diluted from 1:10 to 1:1000 and transferred to a Vero ATCC CCL-81 seeded plate. After letting the inoculum on the cells for 1hr, a viscous methylcellulose overlay was used to prevent the spread of virus to uninfected cells. The cells were allowed to incubate for 44hr before they were fixed and stained with human Mab:E60 and 1:5000 anti-human HRP antibodies and Trueblue Peroxidase Substrate. The plates were then read with a BioSpot Plate Reader.

La Crosse Drug Panel Cell Culture Experiment (Durbadal Ojha)

Vero ATCC CCL-81 cells were plated in a 12-well plate with DMEM medium containing 5% FBS and infected the cells with LACV strain Human/78 at an MOI of 0.5. The infected vero cells were then incubated at 37˚C for 12hr. A panel of compounds was diluted to concentrations of 0.1 μM, 1.0 μM, and 10 μM for NHC and favipiravir from 10 mM stocks and 1.0 μM, 10 μM and 100 μM for ribavirin from a 100 mM stock. After 12hr post infection, the compounds were added to each of the wells, with two replicates for each of the compound concentrations, and two additional wells had DMSO added for vehicle controls. After 36hr post infection, the viral RNA was extracted using QIAamp viral RNA mini kit, which was then sent to our lab for primer ID library preparation. Also after 36hr post infection, the cells were transferred to a black plate and were used in a plaque-forming assay using a protocol similar as previously stated(24).

8E5 Drug Panel Cytotoxicity Experiment (Shuntai Zhou and Collin Hill)

Cultured HIV-1 LAV infected 8E5 cells obtained through the NIH AIDS Reagent Program, Division of AIDS, NIAID, NIH from Dr. Thomas Folks. The 8E5 cells were plated in 12-well plates at $1x10^6$ cells/well and were grown in 90% RPMI 1640 and 10% FBS. The cells were also plated with a panel of drugs, either having 10 μM NHC, 10 μM favipiravir, 100 μM ribavirin, or vehicle control (DMSO), with two replicates of each drug. Every three days, the cells were counted using an Invitrogen Countess automated cell counter, and then changed the media and split the cells to maintain $1x10^6$ cells/well, unless the cell number was below $1x10^6$ cells/well. Additionally, at each of the three day timepoints, the HIV-1 viral RNA was extracted from the cell supernatant of the 10 μM NHC wells, using a QIAamp viral RNA mini kit, which was then used for primer ID library preparation. At the final time point of 21 days, the viral RNA was extracted from the cell

supernatant from each of the wells using the aforementioned method and then used for primer ID library preparation.

MERS-CoV In Vivo Experiment (Timothy Sheahan)

Before infection with MERS-CoV and subsequent treatment with EIDD-2801, equivalent numbers of 10-11 week old C57BL/6J 288/330 DPP4 mice were randomly assigned to each treatment group (5 male/5 female). To control for potential effects associated with oral dosing on animal weight or pulmonary function, as well as the effect of the tested compound, two smaller “sham” infected groups were also included (n = 6, 3 males and 3 females each). EIDD-2801 (500 mg/kg) or vehicle control (10% PEG, 2.5% Cremophor RH40 in water) was delivered via oral gavage (P.O.) twice a day (BID) beginning at -2hr and then every 12 hr thereafter for drug dosing and prophylactic studies. For therapeutic dosing studies, treatment was initiated dosing at -2hr, +12hr, +24hr or +48hr relative to viral infection. Mice were anesthetized with a mixture of ketamine/xylazine prior to intranasal infection with a dose of 5E+04 PFU or 1E+04 PFU MERS p35C4 strain at time 0hr post infection. All mice were weighed daily, and a subset of mice were assayed by whole body plethysmography (4 females per treatment group for MERS-CoV daily to determine pulmonary function. Following sacrifice at 5 days post infection, lung tissue was then removed for virus lung titer and pathology. The large left lobe was harvested for pathology and the lower left lobe was harvested for virus titer.

Primer Design (Collin Hill)

For the Primer ID library preparation, primers were designed using Primer-BLAST (NCBI, NLM, NIH) to target multiple regions found within the different viral genomes and the mice mRNA. The primers were then subsequently tested on various dilutions of viral RNA or mice mRNA using SuperScript III One-Step RT-PCR system (ThermoFisher). The primer pairs that gave the strongest signal at the lowest dilution were then used to make the Primer ID cDNA reverse primers by attaching the reverse adaptor sequence with 11-bp long degenerate nucleotide block (as the Primer ID) and the PCR forward primers by attaching the forward adaptor sequence, as shown in table 1 (15,16,17).

Primer ID Library Preparation (Collin Hill)

From the extracted viral RNA, the cDNA was generated with cDNA primers possessing an 11 bp long block of degenerate nucleotides by using Superscript III kit (ThermoFisher). For MERS-CoV, cDNA primers nsp10_PID11, nsp12_PID11, and nsp14_PID11 were multiplexed for the cell culture sequencing and primers nsp10_PID11, ifit3_PID11, and isg15_PID11 were multiplexed for the in vivo

sequencing. For the ZKV cell culture sequencing, cDNA primers ns3_PID11 and ns5_PID11 were multiplexed. For the LACV cell culture sequencing, cDNA primers L_PID11 and M_PID11 were multiplexed. For the 8E5 cell culture sequencing, just cDNA primer IN4752_PID11 was used. After Agencourt RNAClean XP bead wash purification, the cDNA was amplified by PCR using a mixture of forward primers and a universal reverse primer, followed by a second round of PCR to incorporate Illumina sequencing adaptors and barcodes. After gel-purification of the amplified libraries through Qiagen MinElute Gel Extraction kit and quantification using a Qubit fluorometer, the amplified libraries were pooled and sent to UNC high through-put sequencing facility for Illumina MiSeq 300 bp pair-ended sequencing (15,16,17).

Table 1. Primers used for MiSeq Library prep

Primer	5'-3'	Comment
nsp10_PID11	GTGACTGGAGTTCAGACGTGTGCTCTTCCGATCTNNNNNNNNNNCAGTCCTAAAGACGACATCAGTGG	cDNA primer. Targeting MERS-CoV nsp10 gene.
nsp12_PID11	GTGACTGGAGTTCAGACGTGTGCTCTTCCGATCTNNNNNNNNNNCAGTATAGCCAAAGACACAAACCG	cDNA primer. Targeting MERS-CoV nsp12 gene.
nsp14_PID11	GTGACTGGAGTTCAGACGTGTGCTCTTCCGATCTNNNNNNNNNNCAGTGAACATCGACAAAGAAAGGG	cDNA primer. Targeting MERS-CoV nsp14 gene.
ns3_PID11	GTGACTGGAGTTCAGACGTGTGCTCTTCCGATCTNNNNNNNNNNCAGCTTCCACTTCGGTGTCCATA	cDNA primer. Targeting ZKV ns3 gene.
ns5_PID11	GTGACTGGAGTTCAGACGTGTGCTCTTCCGATCTNNNNNNNNNNCAGGAGGTCCCTTCTGTGGAAAT	cDNA primer. Targeting ZKV ns5 gene.
L_PID11	GTGACTGGAGTTCAGACGTGTGCTCTTCCGATCTNNNNNNNNNNCAGTTCCTGTGGGTAGAGGATAGG	cDNA primer. Targeting LACV RdRp gene found on the large genomic fragment.
M_PID11	GTGACTGGAGTTCAGACGTGTGCTCTTCCGATCTNNNNNNNNNNCAGTAATCCGATAGATGTCCCAGC	cDNA primer. Targeting LACV medium genomic fragment.
ifit3_PID11	GTGACTGGAGTTCAGACGTGTGCTCTTCCGATCTNNNNNNNNNNCAGTTTCAGCCACTCCTTTATCCC	cDNA primer. Targeting mice IFIT3 mRNA.
isg15_PID11	GTGACTGGAGTTCAGACGTGTGCTCTTCCGATCTNNNNNNNNNNCAGTGGGGCTTTAGGCCATACTC	cDNA primer. Targeting mice ISG15 mRNA.
IN4752_PID11	GTGACTGGAGTTCAGACGTGTGCTCTTCCGATCTNNNNNNNNNNATCGAATACTGCCATTTGTACTGC	cDNA primer. Targeting HIV-1 Integrase gene.
nsp10_AD	GCCTCCCTCGCGCCATCAGAGATGTGTATAAGAGACAGNNNNTGCTCAGGTGCTAAGCGAAT	1st round PCR forward primer. Targeting MERS-CoV nsp10 gene.
nsp12_AD	GCCTCCCTCGCGCCATCAGAGATGTGTATAAGAGACAGNNNNATAGGCTTCGATGTTGAGGG	1st round PCR forward primer. Targeting MERS-CoV nsp12 gene.

nsp14_AD	GCCTCCCTCGCGCCATCAGAGATGTGTATAAGAGACAGNNNNATTGCAAGCTGGTTCTAACA	1st round PCR forward primer. Targeting MERS-CoV nsp14 gene
ns3_AD	GCCTCCCTCGCGCCATCAGAGATGTGTATAAGAGACAGNNNNTGGGAAAACCAGGAGAGTTC	1st round PCR forward primer. Targeting ZKV ns3 gene.
ns5_AD	GCCTCCCTCGCGCCATCAGAGATGTGTATAAGAGACAGNNNNACCTAGTGGTGCAACTCATT	1st round PCR forward primer. Targeting ZKV ns5 gene.
L_AD	GCCTCCCTCGCGCCATCAGAGATGTGTATAAGAGACAGNNNNAAGGCCAGAAAACGTCAAAG	1st round PCR forward primer. Targeting LACV RdRp gene found on the large genomic fragment.
M_AD	GCCTCCCTCGCGCCATCAGAGATGTGTATAAGAGACAGNNNNTCCTGACGTAAAGCTCATCC	1st round PCR forward primer. Targeting LACV medium genomic fragment.
isg15_AD	GCCTCCCTCGCGCCATCAGAGATGTGTATAAGAGACAGNNNNTGGGACCTAAAGGTGAAGATG	1st round PCR forward primer. Targeting mice ISG15 mRNA.
ifit3_AD	GCCTCCCTCGCGCCATCAGAGATGTGTATAAGAGACAGNNNNCGATCCACAGTGAACAACAG	1st round PCR forward primer. Targeting mice IFIT3 mRNA.
IN4383_AD	GCCTCCCTCGCGCCATCAGAGATGTGTATAAGAGACAGNNNNAAAAGGAGAAGCCATGCATG	1st round PCR forward primer. Targeting HIV-1 Integrase gene.
Adapter R	GTGACTGGAGTTCAGACGTGTGCTC	1st round PCR reverse primer
Universal Adapter	AATGATACGGCGACCACCGAGATCTACACGCCTCCCTCGCGCCATCAGAGATGTG	2nd round PCR forward primer with Illumina adapter sequence
Indexed Adapter	CAAGCAGAAGACGGCATACGAGATNNNNNNGTGACTGGAGTTCAGACGTGTGCTC	2nd round PCR reverse primer with Illumina adapter sequence and indices (NNNNNNN)
Old Nextera	GCCTCCCTCGCGCCATCAGAGATGTGTATAAGAGACAG	Customized sequencing primer

Bioinformatics and Statistical Analysis (Collin Hill)

The initial primer ID data was processed using the Illumina bcl2fastq pipeline (version 2.0.0) and then the template consensus sequences (TCSs) were constructed using the Swanstrom lab TCS pipeline version 1.3.8 (https://github.com/SwanstromLab/PID). If multiple primers were used, the sequences of each region in the pool were de-multiplexed. RUBY package viral_seq version 1.0.6 (https://rubygems.org/gems/viral_seq) was then used to calculate the mutation rate at each position of each virus with different mutagenic compounds. The data was then analyzed using GraphPad Prism software to make figures and to perform one sample student t-tests on each of the sample groups with a $p>0.05$.

Simulation of The Accumulation of Lethal Mutations in MERS-CoV (Shuntai Zhou and Collin Hill)

To better understand the impact of the increased mutation rate of viral RNA genome on the accumulation of deleterious mutations, we performed a simulation to demonstrate the accumulation of stop codons on MERS-CoV orf1ab using the NHC mutation model. In this model, we set A to G and U to C mutation rate as 'x', G to A mutation as '2x' (two-fold of A to G or U to C mutation rate), and C to U mutation as '3x' (three-fold of A to G or U to C mutation rate). Other types of mutations were ignored. We assumed that one replication cycle of MERS-CoV took 24 hours and we simulated the percentage of orf1ab genomes harboring stop codons after 1 cycle (24 hours) and 5 cycles (5 days) viral replication. Ruby in-house script was used to perform the simulation.

Ethics Regulation of Laboratory Animals (Timothy Sheahan)

Efficacy studies were performed in animal biosafety level 3 facilities at UNC Chapel Hill. All works were conducted under protocols approved by the Institutional Animal Care and Use Committee at UNC Chapel Hill (IACUC protocol #16-284) according to guidelines set by the Association for the Assessment and Accreditation of Laboratory Animal Care and the U.S. Department of Agriculture.

Results

NHC Exhibits Antiviral and Mutagenic Effects in MERS-CoV Cell Culture.

To better understand the effects of these compounds on MERS-CoV, infected cells were cultured with a panel of compounds at various concentrations and after 36 hours, a nano-luciferase assay was done to measure antiviral effects and the viral RNA was extracted and sequenced using multiplexed primers to determine mutagenic effects. NHC was the only compound that was found to have antiviral effects, with a viral titer log decrease of 3.19 at a maximum dosage concentration of 10 μM, while neither ribavirin or favipiravir showed no significant antiviral effects (figure 1A). Similarly, NHC was the only compound that was found to have mutagenic effects, with a 8.76 fold increase in the total error rate and a 35.89 fold increase of the C to U transition rate for the NSP12 primer region at a maximum dosage concentration of 10 μM (figures 1B and 1C). Likely due to this increased mutation rate, in the NSP12 primer region, the 10 μM NHC dosage concentration also increased the proportion of the viral population that had codon changes, with a 3.05 fold increase in the percent of TCS with stop codons and a 6.97 fold increase in the percent of TCS with other codon changes (figures 1D and 1E). Ribavirin and favipiravir did not exhibit any significant codon changes in the TCS. The NSP10 and NSP14 primer regions also exhibited similar results for the mutation rates and codon changes for each of the three compounds (supplemental figures 2 and 3).

Figure 1. MERS-CoV Drug Panel Antiviral Activity and Mutagenic Effects

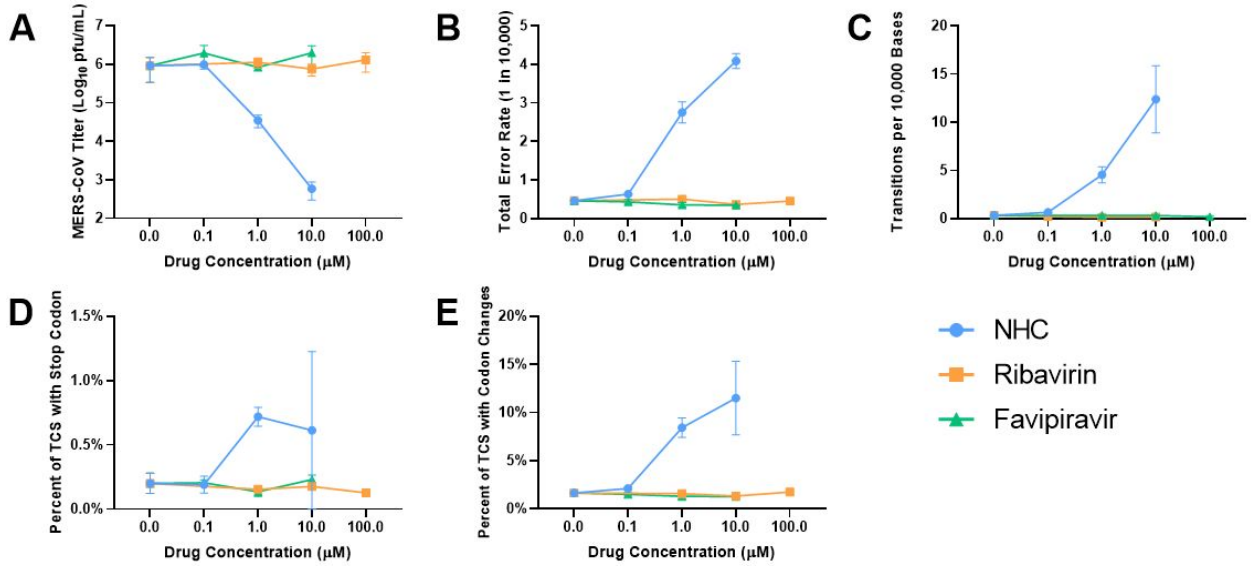

Panel A: MERS-CoV titer as determined from nanoluciferase assay. Panel B: Total error rate (error per 10,000) of NSP12 primer region of MERS-CoV under different compound and concentration conditions. Panel C: Cytidine to uracil (C to U) transition error rate (per 10,000) of NSP12 primer region of MERS-CoV in the drug panel. Panel D: Percent of template consensus sequences (TCS) with a change in codon to UAG, UAA, and UGA (stop codons) within the NSP12 primer region of MERS-CoV. Panel E: Percent of TCS with a change in codon (other than stop codons) within the NSP12 primer region of MERS-CoV. For all panels, the error bars indicate the range of each data set.

<u>NHC Exhibits Antiviral and Mutagenic Effects in Zika Virus Cell Culture.</u>

To investigate if the compounds had similar antiviral and mutagenic effects in Zika virus, infected cells were cultured with a panel of compounds at various concentrations and after 36 hours, a plaque-forming assay was done to measure antiviral effects and the viral RNA was extracted and sequenced using multiplexed primers to determine mutagenic effects. Similar to the results in MERS-CoV, NHC was the only compound that exhibited any significant antiviral effects, although to a much less extent as at a maximal dosage concentration of 10 μM, there was a viral titer log decrease of 0.77 (figure 2A). Also similar to MERS-CoV, NHC was the only compound that exhibited mutagenic effects with a 3.02 fold increase in the total error rate and a 15.70 fold increase in the C to U transition rate for the NS5 primer region at a maximum dosage of 10 μM (figures 2B and 2C). In the NS5 primer region, the 10 μM NHC dosage

concentration also increased the proportion of the viral population that had codon changes, with a 5.70 fold increase in the percent of TCS with stop codons and a 2.31 fold increase in the percent of TCS with other codon changes (figures 2D and 2E). Ribavirin and favipiravir did not exhibit any significant codon changes in the TCS. The NS3 primer regions also exhibited similar results for the mutation rates and codon changes for each of the three compounds (supplemental figure 4).

Figure 3 Zika Virus Drug Panel Antiviral Activity and Mutagenic Effects

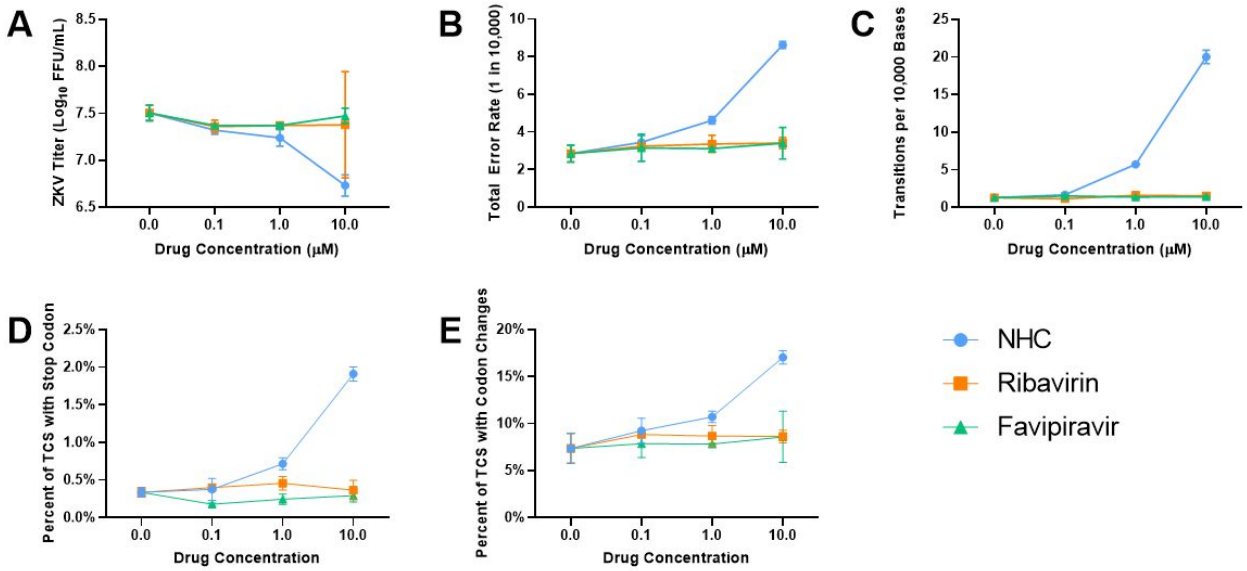

Panel A: Zika virus titer as determined from plaque-forming assay. Panel B: Total error rate (error per 10,000) of NS5 primer region of Zika virus under different compound and concentration conditions. Panel C: Cytidine to uracil (C to U) transition error rate (per 10,000) of NS5 primer region of Zika virus in the drug panel. Panel D: Percent of template consensus sequences (TCS) with a change in codon to UAG, UAA, and UGA (stop codons) within the NS5 primer region of Zika virus. Panel E: Percent of TCS with a change in codon (other than stop codons) within the NS5 primer region of Zika virus. For all panels, the error bars indicate the range of each data set.

<u>NHC, Ribavirin, and Favipiravir Exhibit Antiviral and Mutagenic Effects in La Crosse Virus Cell Culture.</u>

To compare the antiviral and mutagenic effects of the compounds on MERS-CoV and Zika virus to La Crosse virus, infected cells were cultured with a panel of compounds at various concentrations and after 36 hours, a plaque-forming assay was done to measure antiviral effects and the viral RNA was extracted and sequenced using multiplexed primers to determine mutagenic effects. Different from the other two

viruses, all three compounds were found to have antiviral effects to varying degrees. At 10 μM of NHC, there was a 8.06 log decrease in the viral titer and at 100 μM, there was a 9.63 log decrease in the viral titer, causing almost no plaque to form (figure 4a). At maximum dosage concentrations of 100 μM, ribavirin and favipiravir caused 2.70 log and 3.60 log decrease of viral titer, respectively (figure 4a). NHC also had the highest increase in the total error rate, with a 11.54 fold increase at 10 μM and a 11.89 fold increase at 100 μM, indicating that the mutagenic effects plateau above 10 μM (figure 4B). The C to U transition error rate of NHC at 10 μM and 100 μM were increased by 59.20 fold and 64.81 fold, respectively (figure 4C). Differing from the previous two viruses, ribavirin and favipiravir were found to exhibit mutagenic effects, although only at the maximum dosage concentration of 100 μM. Ribavirin increased the total error rate by 3.20 fold and the C to U transition rate by 10.65 fold (figures 4B and 4C). Favipiravir increased the total error rate by 1.29 fold and the C to U transition rate by 3.57 fold (figures 4B and 4C). NHC also increased the proportion of the population that had codon changes, with a maximum change found at the 10 μM dosage concentration, with a 265.4 fold increase in the percent of TCS with stop codons and a 6.2 fold increase in the percent of TCS with other codon changes (figures 4D and 4E). At a 100 μM dosage concentration of NHC, there was a 258.6 fold increase in the percent of TCS with stop codons and a 5.7 fold increase in the percent of TCS with other codon changes (figures 4D and 4E). At a dosage concentration of 100 μM, ribavirin was also found to increase codon changes, with a 68.0 fold increase in the percent of TCS with stop codons and a 2.5 fold increase in the percent of TCS with other codon changes (figures 4D and 4E). Similarly, at a dosage concentration of 100 μM, favipiravir was found to increase codon changes, with a 68.7 fold increase in the percent of TCS with stop codons and a 1.87 fold increase in the percent of TCS with other codon changes (figures 4D and 4E).

Figure 4. La Crosse Virus Drug Panel Antiviral and Mutagenic Effects

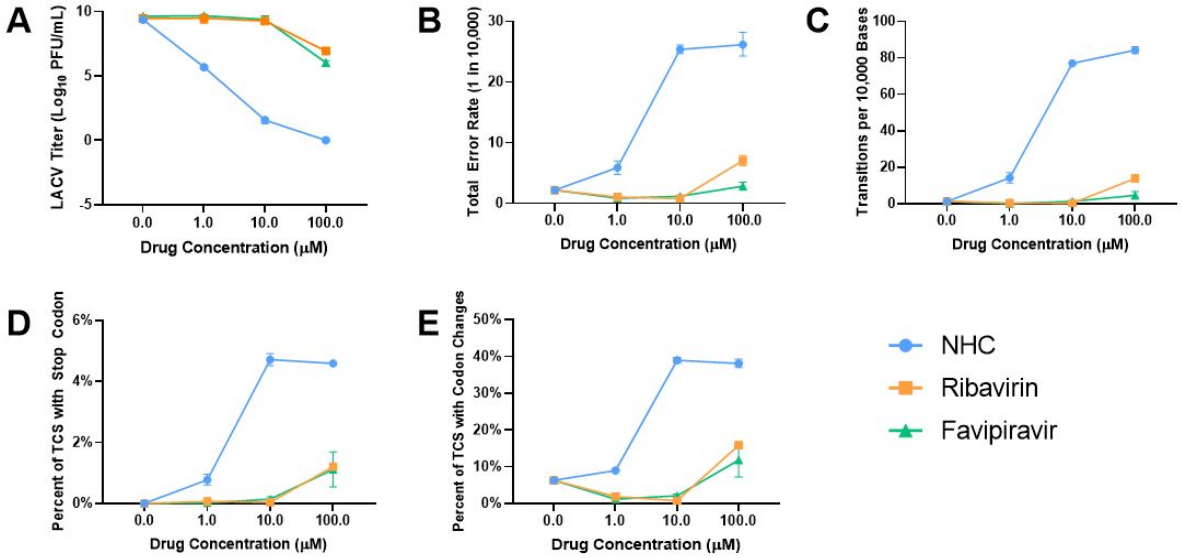

Panel A: La Crosse virus titer as determined from plaque-forming assay. Panel B: Total error rate (error per 10,000) of L fragment primer region of La Crosse virus under different compound and concentration conditions. Panel C: Cytidine to uracil (C to U) transition error rate (per 10,000) of L fragment primer region of La Crosse virus in the drug panel. Panel D: Percent of template consensus sequences (TCS) with a change in codon to UAG, UAA, an UGA (stop codons) within the L fragment primer region of La Crosse virus. Panel E: Percent of TCS with a change in codon (other than stop codons) within the L fragment primer region of La Crosse virus. For all panels, the error bars indicate the range of each data set.

<u>Cytotoxicity and Mutagenicity of NHC, Ribavirin, and Favipiravir in 8E5 Cell Culture.</u>
The cell toxicity assay utilized 8E5 cells, all hosting one copy of the same defective proviral HIV. These cells were cultured for 21 days with either vehicle control (DMSO), 10 µM NHC, 10 µM Favipiravir, or 100 µM Ribavirin. Every three days, in addition to the drugs and media being replaced, the cells were counted and the viral RNA was extracted and sequenced using multiplexed primers to determine mutagenic effects. Based on observations of the cell count, favipirairavir had the same cytotoxicity as the vehicle control and NHC was slightly more cytotoxic (figure 5a). Ribavirin, however, was significantly more cytotoxic and inhibited cell growth (figure 5a). At day 21, NHC was also found to increase the total error rate by 2.9 fold, the C to T transition error rate by 2.7 fold, and the T to C transition error rate by 3.0 fold in the integrase primer region of the proviral HIV (figure 5c). At day 21, ribavirin and favipiravir were not found to noticeably increase the total error rate or increase the transition or transversion

mutation rates (figure 5c). NHC was found to have a plateaued maximum total error rate that stayed consistent between days 6 through 15 (figure 5b).

Figure 5 8E5 Cell Toxicity Assay

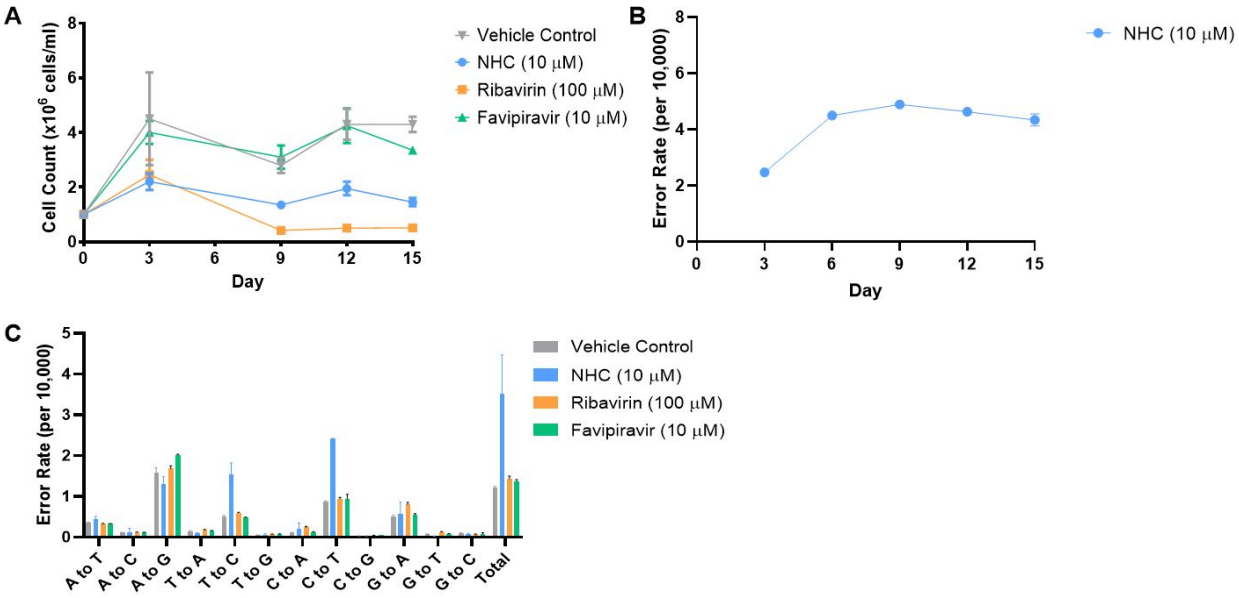

Panel A: Cell count of the 8E5 cells cultured with vehicle control, NHC (10 μM), ribavirin, (100 μM), or favipiravir (10 μM) over 15 days. Panel B: Total error rate of 8E5 cells cultured with NHC (10 μM) between day 3 and day 15 using data from the integrase primer region of HIV-1. Panel C: Mutagenic profile of 8E5 cells cultured with vehicle control, NHC (10 μM), ribavirin, (100 μM), or favipiravir (10 μM) at day 21 using integrase primer region of HIV-1.

<u>NHC Prodrug (EIDD-2801) Exhibits Antiviral and Mutagenic Effects in MERS-CoV Mice Model with Limited Mutagenic Effects on Mice.</u>

The in vivo experiments were completed in mouse models that were infected with MERS-CoV. The mice were treated by giving them either vehicle control or EIDD-2801 at a dosage of 500 mg/kg twice per day, but their dosing regimen was started at different times (-2 hr, +12 hr, +24 hr, +48 hr from time of infection). Viral RNA and murine mRNA was then extracted and sequenced. The sequencing results include three sets of multiplexed primers that contain fragments within NSP10, a nonstructural protein coding region of MERS-CoV (also used for the MERS-CoV in vitro studies), and ISG15 and IFIT3, two genes that are highly expressed in mice during MERS-CoV infection. The template consensus sequence numbers of the various dosing regimens of EIDD-2801 (figure 6A) strongly correlated with the decrease in the viral titres found

within the mice (data not shown), indicating significant antiviral effects for -2 hr BID and +12 hr BID dosing regimens. For dosing regimens starting prior to infection and up to 24 hr post infection, there was a significant increase in both the total error rate (figure 6C and figure 6D), with a 6.0 fold increase at -2 hr BID, a 5.4 fold increase at +12 hr BID, and a 3.4 fold increase at +24 hr BID for the NSP10 primer region of MERS-CoV. It was also observed that there was a correlation between this increase in error rates with the increase in the percent of the TCS, representative of the viral population, with non-synonymous codon changes (figure 6B), which for a highly conserved protein like NSP10, are likely deleterious and lethal codon changes. It was also observed that there was a limited detection of off-target mutations found within the ISG-15 and IFIT-3 primer regions, indicating that EIDD-2801 does not significantly increase the transcriptional error rate or the DNA replication error rate of mice at the dosage concentration given (figure 6C and figure 6D).

Figure 6 In Vivo MERS-CoV in Mice Model with Oral NHC Prodrug

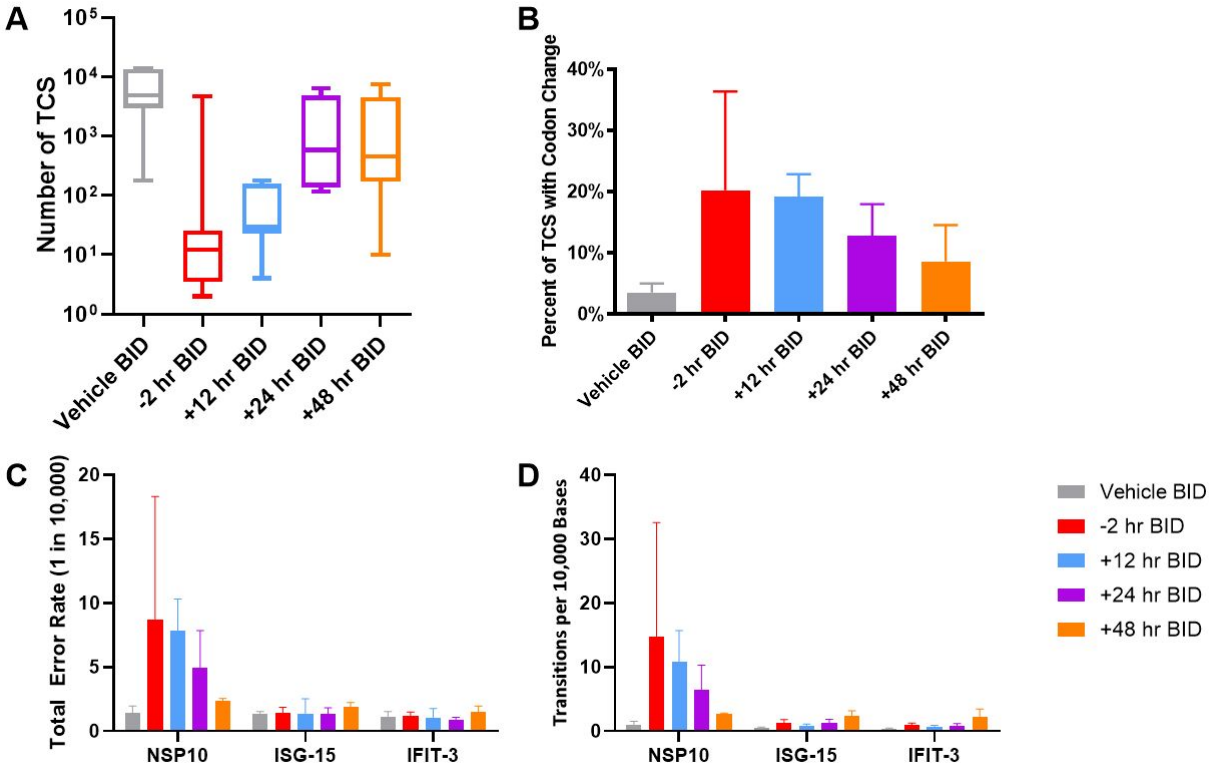

Panel A: Total template consensus sequences (TCS) of the NSP10 primer region of MERS-CoV. The TCS number can act as a proxy representation of the viral load of MERS-CoV within the mice. Panel B: Percent of the TCS with some type of codon change (including stop codons) of the NSP10 primer region of MERS-CoV. Panel C: Total error rate (errors per 10,000) of the NSP10 primer region of MERS-CoV and the

ISG-15 and IFIT-3 primer regions of mice mRNA. Panel D: Shows the Cytidine to Uracil (C to U) transition error rate (per 10,000) of the NSP10 primer region of MERS-CoV and the ISG-15 and IFIT-3 primer regions of mice mRNA. For all panels, the error bars indicate the range of each data set.

Simulation of NHC Exhibits Relationship Between Increase in Error Rate and The Accumulation of Lethal Mutations in MERS-CoV Viral Population

We simulated the percentage of MERS-CoV orf1ab without stop codons, or otherwise intact genomes, using the NHC model described in the methods. We found that in the simulated viral population at an error rate found at 10 μM NHC, only 32% of the orb1ab genomes had no stop codons in the reading frame after only one cycle of replication (one day). Furthermore, after five cycles (five days) of replication, almost all the viral genomes at orb1ab had stop codons. When we used the error rate found at 0.1 μM NHC, we found 61% and 8.4% of the genomes without stop codons at orf1ab after one and five cycles, respectively (Figure 7). This simulation demonstrated that with even a slight increase in the error rate during the viral RNA replication, deleterious mutations will accumulate very quickly, leading to the diminishing of the virus, supporting the concept of lethal mutagenesis as an antiviral mechanism.

Figure 7. Simulation of percentage of MERS-CoV orf1ab without stop codons using an NHC mutation model.

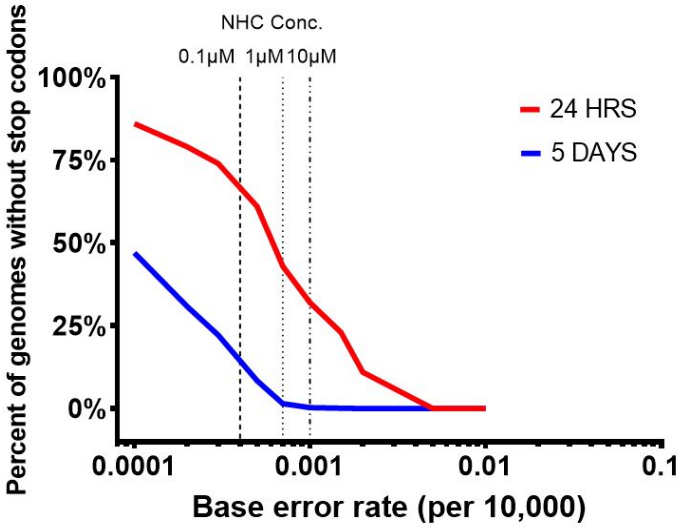

Discussion

In this study, we show a head-to-head comparison three potential mutagenic compounds (N4-beta-hydrocytidine, Favipiravir, and Ribavirin) on a panel of RNA

viruses grown in cell culture, including Middle Eastern Respiratory Syndrome coronavirus (MERS-CoV), Zika virus (ZIKV), and La Crosse virus (LACV). To examine the antiviral activity of these three compounds, we used infectivity assays on each of the viruses and then to examine the mutagenic effects of the compounds, we used primer ID next-generation sequencing (NGS). This deep sequencing approach allows for deep coverage of the viral population and corrects for both PCR resampling and recombination and allows for the creation of a template consensus sequence (TCS) by aligning all sequences with the same primer ID, greatly reducing the method error rate caused by PCR and high throughput sequencing (15,16). Thus, this sequencing approach allows for the highly accurate determination of viral mutation rates and validates the detection of rare viral mutants. To examine the cytotoxicity of each of the three compounds, we measured the effects of the compounds on cell growth in an 8E5 cell model, which harbors a single HIV provirus per cell. We also used this cell model to monitor the effects of these compounds on transcriptional error rates and DNA replication error rates by using primer ID NGS to sequence the expressed HIV viral RNA. We also used an in vivo mice-MERS coronavirus model to study the antiviral effects and short-term toxicity of NHC in vivo by using a novel approach to sequence both the viral RNA as well as the mice mRNA simultaneously through multiplexing with different primers.

MERS-CoV belongs to the genus betacoronavirus, the same genus as Severe Acute Respiratory Syndrome (SARS) coronavirus, the virus which caused the 2002 SARS epidemic, and in the same genus as SARS-CoV-2, the virus which is causing the recent pandemic of COVID-19 (3,13). MERS-CoV emerged in the middle east back in 2012, but has continued to infect patients since then (13). Currently, there is no vaccine or effective antiviral treatment for MERS-CoV, although there have been some recent studies that shows that remdesivir (GS-5734), a small molecule, nucleoside analog, has the potential to be effective in the clinical treatment of this infectious disease (25). Ribavirin has been previously tested on MERS-CoV and was proven to be ineffective, citing NSP14 (an 3’ to 5’ exonuclease) activity to be a proofreading mechanism that prevented the misincorporation of ribavirin.(13,26). NHC has also been previously tested on MERS-CoV, however in comparison to ribavirin, its results were much more promising, as it was found to exhibit significant antiviral activity, despite MERS-CoV’s proofreading activity (13) In this previous study of NHC, its exact mechanism of action was not confirmed and was only suggested that it could act through lethal mutagenesis (13). In our MERS-CoV cell culture experiment, we compared the antiviral and mutagenic effects of ribavirin and NHC and found similar results to previous experiments, where ribavirin failed to exhibit antiviral or mutagenic effects and NHC was found to be a potent antiviral to MERS-CoV and we were able to observe significant

mutagenic effects, providing further support that NHC's mechanism of action is through lethal mutagenesis. Favipiravir has not been tested previously on MERS-CoV, but in our cell culture experiment, it failed to exhibit any antiviral or mutagenic effects, potentially due to MERS-CoV's proofreading activity or due to cell-mediated drug resistance (27,28,29). Additionally, we examined an orally bioavailable NHC prodrug, EIDD-2801, in a MERS-CoV mouse model and we observed similar results as the cell culture experiment, where the NHC prodrug exhibited significant antiviral and mutagenic effects on MERS-CoV. Due to EIDD-2801's oral bioavailability, it is able to be more accessible in clinical settings when compared to intravenous drugs as it could be administered in pill form. According to NHC's results in cell culture and the NHC prodrug's results in vivo, this drug shows promise as a clinical treatment for not only for MERS-CoV, but also potentially for other RNA viruses (30), including other coronaviruses.

Of a different genus than MERS-CoV, Zika virus (ZIKV) belongs to the genus flavivirus, the same genus as Dengue virus (DENV), West Nile virus (WNV), and yellow fever virus (YFV) (31). The last major outbreak of ZIKV was between 2015 and 2016 in the Americas, and infected more than 700,000 people (32). Currently, there is no effective antiviral treatment for ZIKV, however previous studies have shown favipiravir to be effective against ZIKV in cell culture (33,34) and ribavirin to be effective against ZIKV in cell culture and in mouse models (33,35), although the exact mechanism of action of these drugs on ZIKV has yet to be characterized. In our ZIKV cell culture experiment, we did not observe any antiviral or mutagenic effects exhibited by either ribavirin or favipiravir, but this could be due to cell-mediated drug resistance against these two compounds from the vero cells that we used (27,28,29). NHC has not been previously tested on ZIKV, however from our ZIKV cell culture experiment, we found that NHC exhibited significant antiviral and mutagenic effects on ZIKV, indicating that NHC acts through lethal mutagenesis as an antiviral mechanism against ZIKV by being misincorporated by ZIKV's RNA-dependent RNA polymerase.

The third virus we examined, La Crosse virus (LACV), is considerably different from the other two viruses that we examined. Unlike MERS-CoV and ZIKV, which both have non-segmented positive-sense RNA genomes (36,37), LACV, similar to other viruses in the genus orthobunyavirus, has a negative-sense RNA genome that is segmented into three different fragments (38). On average, there are 68 new cases of La Crosse encephalitis neuroinvasive disease caused by LACV each year in the US, mostly occurring around Appalachia in the eastern portion of the US (39). Currently, there is no vaccine nor specific antiviral treatment for LACV, however ribavirin and favipiravir have both previously been shown to be effective against a variety of bunyaviruses in cell culture, including La Crosse virus (40), although their antiviral

mechanisms in bunyaviruses are not fully characterized. In our cell culture experiment with LACV, we found similar antiviral effects of ribavirin and favipiravir on LACV. Additionally, we were able to detect the mutagenic effects of these compounds on LACV, providing evidence that these two compounds acted through lethal mutagenesis. NHC has not been tested on LACV or any other bunyavirus before, however our LACV cell culture experiment shows that NHC is a much more potent antiviral against LACV than the other two compounds. We also found that NHC exhibited mutagenic effects, providing support that NHC exhibited its antiviral effects through a mechanism of lethal mutagenesis.

From the Primer ID NGS results, we can observe that favipiravir and NHC both primarily increase G to A and C to U transitions and to a lesser extent, increase A to G and U to C transitions (see supplemental figure 1). This increase in transition error rates is consistent with previous findings for each of the drugs (30,41) and provides support that both of the compounds act as purine analogs, allowing them to bind primarily to guanosine but also to adenosine to induce mutations when incorporated by the viral RNA-dependent RNA polymerase (RDRP)(see supplemental table 1). We also observed that in LACV cell culture, ribavirin increased the G to A and C to U transition rates, and slightly increased the A to G and C to U transition rates (see supplemental figure 1), which is also consistent with previous literature (42,43,44). However, ribavirin is different from the other two compounds, in that it acts as a pyrimidine analog and can bind to either cytidine or uridine, which is how it induces mutations whenever it is incorporated by viral RDRP (43).

In the 8E5 cytotoxicity experiment, the lack of significant cytotoxicity by favipiravir at 10 μM is consistent with previous findings, where even at concentrations greater than 1,000 μM, there were no significant signs of cytotoxicity (41). The relatively high cytotoxicity of ribavirin at 100 μM is also consistent with previous research as the CC_{50} has been shown in some studies to be anywhere between 30 μM to over 100 μM (44,45). The cytotoxicity of NHC at 10 μM was found to be somewhat intermediate between ribavirin and favipiravir, where the CC_{50} can range anywhere between 10 μM to over 200 μM (13,30,46). In the MERS-CoV mouse model experiment with EIDD-2801, which will be converted into NHC in vivo, there were no significant toxic effects observed and there was not a significant increase in the error rate of the upregulated mice genes, whether caused by DNA mutations or transcriptional mutations (figures 6C and 6D). These results directly contrasted with the results that we observed with NHC in the 8E5 cell culture experiment, as we found that NHC caused a significant increase in the error rate of the expressed HIV (figure 5C). However, it is likely that this increase in error rate caused by NHC arises from an increase in the transcriptional error rate rather

than an increase in the DNA mutations. As seen in figure 5C, the C to T and T to C transition error rates for NHC were the only mutations that increased significantly. Both of these mutations can only be caused by the misincorporation of NHC in the positive-sense strand of the DNA genome or by the misincorporation of NHC during transcription. No significant increase of mutations were observed from the misincorporation of NHC in the negative-sense strand of the DNA genome (G to A or A to G transitions). This indicates that the errors are coming from transcriptional errors caused by the misincorporation of NHC by the DNA-dependent RNA polymerase (host RNA polymerase II) rather than DNA replication errors caused by the misincorporation of NHC by the DNA-dependent DNA polymerase, as then we would observe equal rates of positive-sense misincorporation and negative-sense misincorporation transition errors. Also, as seen by figure 5B, the error rate of the 8E5 cells with NHC plateaued after day 6, which further supports that the increase in error rate arises from transcriptional errors as we would likely observe a gradual increase of the error rate over time if there were significant levels of DNA mutations caused by NHC. These findings are consistent with another study that has found NHC to increase the rate of transcriptional errors caused by mitochondrial DNA-dependent RNA polymerase (46). We did not observe a transcriptional error rate in the mice in vivo experiment, likely due to the therapeutic concentration of NHC was much lower than in the 8E5 cell culture. However, this does not prove that there are no DNA mutations caused by NHC, as more experimentation is needed to prove the absence of DNA mutations before NHC can be tested in humans due to risk for carcinogenicity. It is possible that the cytotoxic effects of NHC are caused by the increase in the transcriptional error rate, as mutated nuclear mRNA and mutated mitochondrial mRNA can have codon changes that result in cellular proteins that have altered function or loss of function that contribute to cytotoxic effects (46, 47).

In conclusion, we found Primer ID NGS was a useful tool to screen mutagenic compounds as antiviral drugs. We found that NHC was a broad-spectrum antiviral drug by increasing the transition mutation rate in the viral genome, however NHC exhibits cytotoxic effects in cell culture, likely by increasing the transcriptional error rate of the host cells. Additionally, we found that the NHC prodrug, EIDD-2801, was effective against MERS-CoV in vivo with no significant cytotoxic effects observed, showing promise that this NHC prodrug could be used clinically to treat RNA viral infectious diseases.

Acknowledgments

I would like to thank all members of Swanstrom lab, especially Shuntai Zhou and Ronald Swanstrom for providing mentorship and guidance on this project, and Sabrina Clark for helping with some of the primer ID library preparation. I would also like to thank Timothy Sheahan from Baric lab for their work on the MERS-CoV cell culture and mouse model experiments, Derek Carbaugh from Lazear lab for their work on the ZIKV cell culture experiment, and Durbadal Ojha from Peterson lab at NIAID Rocky Mountain laboratories for their work on the LACV cell culture experiment. I would also like to thank George Painter from Emory Institute for Drug Discovery for providing EIDD-2801 and Ray Schinazi from NIH AIDS Reagent Program for providing N4-beta-hydroxycytidine for testing.

References

1. Rosenberg R. Detecting the emergence of novel, zoonotic viruses pathogenic to humans. Cellular and Molecular Life Sciences. 2014;72(6):1115–1125. doi:10.1007/s00018-014-1785-y
2. Carrasco-Hernandez R, Jácome R, Vidal YL, León SPD. Are RNA Viruses Candidate Agents for the Next Global Pandemic? A Review. ILAR Journal. 2017;58(3):343–358. doi:10.1093/ilar/ilx026
3. Lai C-C, Shih T-P, Ko W-C, Tang H-J, Hsueh P-R. Severe acute respiratory syndrome coronavirus 2 (SARS-CoV-2) and coronavirus disease-2019 (COVID-19): The epidemic and the challenges. International Journal of Antimicrobial Agents. 2020:105924. doi:10.1016/j.ijantimicag.2020.105924
4. Kim H, Ellis VD, Woodman A, Zhao Y, Arnold JJ, Cameron CE. RNA-dependent RNA polymerase speed and fidelity are not the only determinants of the mechanism or efficiency of recombination. 2019. doi:10.1101/769224
5. Graci JD, Cameron CE. Therapeutically targeting RNA viruses via lethal mutagenesis. Future Virology. 2008;3(6):553–566. doi:10.2217/17460794.3.6.553
6. Plotkin S, Robinson JM, Cunningham G, Iqbal R, Larsen S. The complexity and cost of vaccine manufacturing – An overview. Vaccine. 2017;35(33):4064–4071. doi:10.1016/j.vaccine.2017.06.003
7. Choi KH. Viral Polymerases. Viral Molecular Machines Advances in Experimental Medicine and Biology. 2011 Aug:267–304. doi:10.1007/978-1-4614-0980-9_12
8. Sanjuán R. Viral Mutation Rates. Virus Evolution: Current Research and Future Directions. 2016:1–28. doi:10.21775/9781910190234.01

9. Freistadt M. Lethal mutagens: broad-spectrum antivirals with limited potential for development of resistance? Drug Resistance Updates. 2004;7(1):19–24. doi:10.1016/j.drup.2003.12.003
10. Elena SF, Sanjuan R. Adaptive Value of High Mutation Rates of RNA Viruses: Separating Causes from Consequences. Journal of Virology. 2005;79(18):11555–11558. doi:10.1128/jvi.79.18.11555-11558.2005
11. Duarte E, Clarke D, Moya A, Domingo E, Holland J. Rapid fitness losses in mammalian RNA virus clones due to Muller's ratchet. Proceedings of the National Academy of Sciences. 1992;89(13):6015–6019. doi:10.1073/pnas.89.13.6015
12. Bull JJ, Sanjuan R, Wilke CO. Theory of Lethal Mutagenesis for Viruses. Journal of Virology. 2007;81(6):2930–2939. doi:10.1128/jvi.01624-06
13. Agostini ML, Pruijssers AJ, Chappell JD, Gribble J, Lu X, Andres EL, Bluemling GR, Lockwood MA, Sheahan TP, Sims AC, et al. Small-Molecule Antiviral β-D-N4-Hydroxycytidine Inhibits a Proofreading-Intact Coronavirus with a High Genetic Barrier to Resistance. Journal of Virology. 2019;93(24). doi:10.1128/jvi.01348-19
14. Isakov O, Bordería AV, Golan D, Hamenahem A, Celniker G, Yoffe L, Blanc H, Vignuzzi M, Shomron N. Deep sequencing analysis of viral infection and evolution allows rapid and detailed characterization of viral mutant spectrum. Bioinformatics. 2015;31(13):2141–2150. doi:10.1093/bioinformatics/btv101
15. Jabara CB, Jones CD, Roach J, Anderson JA, Swanstrom R. Accurate sampling and deep sequencing of the HIV-1 protease gene using a Primer ID. Proceedings of the National Academy of Sciences. 2011;108(50):20166–20171. doi:10.1073/pnas.1110064108
16. Zhou S, Jones C, Mieczkowski P, Swanstrom R. Primer ID Validates Template Sampling Depth and Greatly Reduces the Error Rate of Next-Generation Sequencing of HIV-1 Genomic RNA Populations. Journal of Virology. 2015;89(16):8540–8555. doi:10.1128/jvi.00522-15
17. Wong KH, Jin Y, Moqtaderi Z. Multiplex Illumina Sequencing Using DNA Barcoding. Current Protocols in Molecular Biology. 2013. doi:10.1002/0471142727.mb0711s101
18. Pauly MD, Lauring AS. Effective Lethal Mutagenesis of Influenza Virus by Three Nucleoside Analogs. Journal of Virology. 2015;89(7):3584–3597. doi:10.1128/jvi.03483-14
19. Furuta Y, Komeno T, Nakamura T. Favipiravir (T-705), a broad spectrum inhibitor of viral RNA polymerase. Proceedings of the Japan Academy, Series B. 2017;93(7):449–463. doi:10.2183/pjab.93.027

20. Gowen BB, Wong M-H, Jung K-H, Sanders AB, Mendenhall M, Bailey KW, Furuta Y, Sidwell RW. In Vitro and In Vivo Activities of T-705 against Arenavirus and Bunyavirus Infections. Antimicrobial Agents and Chemotherapy. 2007;51(9):3168–3176. doi:10.1128/aac.00356-07
21. Sangawa H, Komeno T, Nishikawa H, Yoshida A, Takahashi K, Nomura N, Furuta Y. Mechanism of Action of T-705 Ribosyl Triphosphate against Influenza Virus RNA Polymerase. Antimicrobial Agents and Chemotherapy. 2013;57(11):5202–5208. doi:10.1128/aac.00649-13
22. Feld JJ, Hoofnagle JH. Mechanism of action of interferon and ribavirin in treatment of hepatitis C. Nature. 2005;436(7053):967–972. doi:10.1038/nature04082
23. Cameron CE, Castro C. The mechanism of action of ribavirin: lethal mutagenesis of RNA virus genomes mediated by the viral RNA-dependent RNA polymerase. Current Opinion in Infectious Diseases. 2001;14(6):757–764. doi:10.1097/00001432-200112000-00015
24. Ojha D, Das R, Sobia P, Dwivedi V, Ghosh S, Samanta A, Chattopadhyay D. Pedilanthus tithymaloides Inhibits HSV Infection by Modulating NF-κB Signaling. Plos One. 2015;10(9). doi:10.1371/journal.pone.0139338
25. Sheahan TP, Sims AC, Leist SR, Schäfer A, Won J, Brown AJ, Montgomery SA, Hogg A, Babusis D, Clarke MO, et al. Comparative therapeutic efficacy of remdesivir and combination lopinavir, ritonavir, and interferon beta against MERS-CoV. Nature Communications. 2020;11(1). doi:10.1038/s41467-019-13940-6
26. Chong YP, Song JY, Seo YB, Choi J-P, Shin H-S. Antiviral Treatment Guidelines for Middle East Respiratory Syndrome. Infection & Chemotherapy. 2015;47(3):212. doi:10.3947/ic.2015.47.3.212
27. Franco EJ, Rodriquez JL, Pomeroy JJ, Hanrahan KC, Brown AN. The effectiveness of antiviral agents with broad-spectrum activity against chikungunya virus varies between host cell lines. Antiviral Chemistry and Chemotherapy. 2018;26:204020661880758. doi:10.1177/2040206618807580
28. Shah NR, Sunderland A, Grdzelishvili VZ. Cell Type Mediated Resistance of Vesicular Stomatitis Virus and Sendai Virus to Ribavirin. PLoS ONE. 2010;5(6). doi:10.1371/journal.pone.0011265
29. Ibarra KD, Pfeiffer JK. Reduced Ribavirin Antiviral Efficacy via Nucleoside Transporter-Mediated Drug Resistance. Journal of Virology. 2009;83(9):4538–4547. doi:10.1128/jvi.02280-08
30. Yoon J-J, Toots M, Lee S, Lee M-E, Ludeke B, Luczo JM, Ganti K, Cox RM, Sticher ZM, Edpuganti V, et al. Orally Efficacious Broad-Spectrum

Ribonucleoside Analog Inhibitor of Influenza and Respiratory Syncytial Viruses. Antimicrobial Agents and Chemotherapy. 2018;62(8). doi:10.1128/aac.00766-18
31. Beckham JD, Pastula DM, Massey A, Tyler KL. Zika Virus as an Emerging Global Pathogen. JAMA Neurology. 2016;73(7):875. doi:10.1001/jamaneurol.2016.0800
32. Maslow JN. Zika Vaccine Development—Current Progress and Challenges for the Future. Tropical Medicine and Infectious Disease. 2019;4(3):104. doi:10.3390/tropicalmed4030104
33. Kim J-A, Seong R-K, Kumar M, Shin O. Favipiravir and Ribavirin Inhibit Replication of Asian and African Strains of Zika Virus in Different Cell Models. Viruses. 2018;10(2):72. doi:10.3390/v10020072
34. Mello CPPD, Tao X, Kim TH, Bulitta JB, Rodriquez JL, Pomeroy JJ, Brown AN. Zika Virus Replication Is Substantially Inhibited by Novel Favipiravir and Interferon Alpha Combination Regimens. Antimicrobial Agents and Chemotherapy. 2017;62(1). doi:10.1128/aac.01983-17
35. Kamiyama N, Soma R, Hidano S, Watanabe K, Umekita H, Fukuda C, Noguchi K, Gendo Y, Ozaki T, Sonoda A, et al. Ribavirin inhibits Zika virus (ZIKV) replication in vitro and suppresses viremia in ZIKV-infected STAT1-deficient mice. Antiviral Research. 2017;146:1–11. doi:10.1016/j.antiviral.2017.08.007
36. White MK, Wollebo HS, Beckham JD, Tyler KL, Khalili K. Zika virus: An emergent neuropathological agent. Annals of Neurology. 2016;80(4):479–489. doi:10.1002/ana.24748
37. Fehr AR, Perlman S. Coronaviruses: An Overview of Their Replication and Pathogenesis. Coronaviruses Methods in Molecular Biology. 2015:1–23. doi:10.1007/978-1-4939-2438-7_1
38. Obijeski JF, Bishop DH, Palmer EL, Murphy FA. Segmented genome and nucleocapsid of La Crosse virus. Journal of Virology. 1976;20(3):664–675. doi:10.1128/jvi.20.3.664-675.1976
39. La Crosse Encephalitis: Epidemiology & Geographic Distribution. Centers for Disease Control and Prevention. 2019 Jun 24. https://www.cdc.gov/lac/tech/epi.html
40. Gowen BB, Wong M-H, Jung K-H, Sanders AB, Mendenhall M, Bailey KW, Furuta Y, Sidwell RW. In Vitro and In Vivo Activities of T-705 against Arenavirus and Bunyavirus Infections. Antimicrobial Agents and Chemotherapy. 2007;51(9):3168–3176. doi:10.1128/aac.00356-07
41. Baranovich T, Wong S-S, Armstrong J, Marjuki H, Webby RJ, Webster RG, Govorkova EA. T-705 (Favipiravir) Induces Lethal Mutagenesis in Influenza A H1N1 Viruses In Vitro. Journal of Virology. 2013;87(7):3741–3751. doi:10.1128/jvi.02346-12

42. Crotty S, Cameron C, Andino R. Ribavirin's antiviral mechanism of action: lethal mutagenesis? Journal of Molecular Medicine. 2002;80(2):86–95. doi:10.1007/s00109-001-0308-0
43. Aljabr W, Touzelet O, Pollakis G, Wu W, Munday DC, Hughes M, Hertz-Fowler C, Kenny J, Fearns R, Barr JN, et al. Investigating the Influence of Ribavirin on Human Respiratory Syncytial Virus RNA Synthesis by Using a High-Resolution Transcriptome Sequencing Approach. Journal of Virology. 2015;90(10):4876–4888. doi:10.1128/jvi.02349-15
44. Ortega-Prieto AM, Sheldon J, Grande-Pérez A, Tejero H, Gregori J, Quer J, Esteban JI, Domingo E, Perales C. Extinction of Hepatitis C Virus by Ribavirin in Hepatoma Cells Involves Lethal Mutagenesis. PLoS ONE. 2013;8(8). doi:10.1371/journal.pone.0071039
45. Oestereich L, Rieger T, Neumann M, Bernreuther C, Lehmann M, Krasemann S, Wurr S, Emmerich P, Lamballerie XD, Ölschläger S, et al. Evaluation of Antiviral Efficacy of Ribavirin, Arbidol, and T-705 (Favipiravir) in a Mouse Model for Crimean-Congo Hemorrhagic Fever. PLoS Neglected Tropical Diseases. 2014;8(5). doi:10.1371/journal.pntd.0002804
46. Sticher ZM, Lu G, Mitchell DG, Marlow J, Moellering L, Bluemling GR, Guthrie DB, Natchus MG, Painter GR, Kolykhalov AA. Analysis of the Potential for N4-Hydroxycytidine To Inhibit Mitochondrial Replication and Function. Antimicrobial Agents and Chemotherapy. 2019;64(2). doi:10.1128/aac.01719-19
47. Gout J-F, Li W, Fritsch C, Li A, Haroon S, Singh L, Hua D, Fazelinia H, Smith Z, Seeholzer S, et al. The landscape of transcription errors in eukaryotic cells. Science Advances. 2017;3(10). doi:10.1126/sciadv.1701484

Supplemental Information

Supplemental Figure 1. Mutation Profiles of Drug Panel on La Crosse Virus

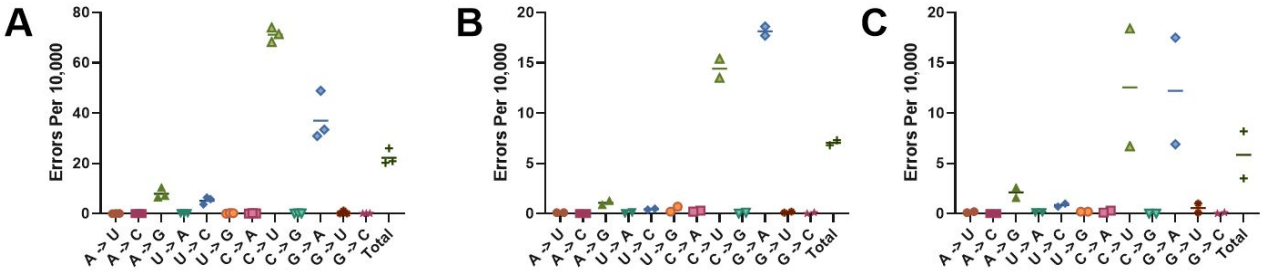

Panel A: NHC mutation profile of L primer region of La Crosse virus. Panel B: Ribavirin mutation profile of L primer region of La Crosse virus. Panel C Favipiravir mutation profile of L primer region of La Crosse virus.

Supplemental Table 1. NHC Binding and Mutation Pattern In Negative-sense RNA Viruses

Input Genomic - RNA	Genomic + RNA	Progeny Genomic - RNA	DNA Amplicon	Genomic Mutation
A	NHC	A	A	
A	NHC	G	G	A to G
G	NHC	G	G	
G	NHC	A	A	G to A
C	G	NHC	C	
C	G	NHC	T	C to U
U	A	NHC	T	
U	A	NHC	C	U to C

Supplemental Figure 2. MERS-CoV NSP10 Primer Region Drug Panel Antiviral Activity and Mutagenic Effects

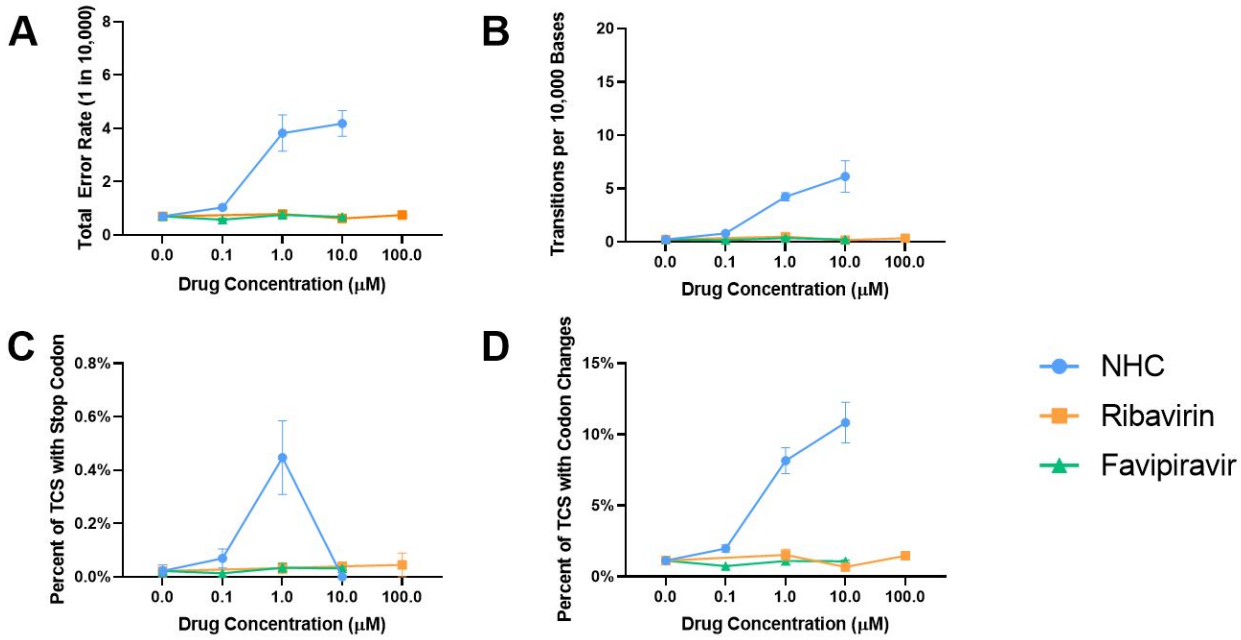

Panel A: Total error rate (error per 10,000) of NSP10 primer region of MERS-CoV under different compound and concentration conditions. Panel B: Cytidine to uracil (C to U) transition error rate (per 10,000) of NSP10 primer region of MERS-CoV in the drug panel. Panel C: Percent of template consensus sequences (TCS) with a change in codon to UAG, UAA, an UGA (stop codons) within the NSP10 primer region of MERS-CoV. Panel D: Percent of TCS with a change in codon (other than stop codons) within the NSP10 primer region of MERS-CoV. For all panels, the error bars indicate the range of each data set.

Supplemental Figure 3. MERS-CoV NSP14 Primer Region Drug Panel Antiviral Activity and Mutagenic Effects

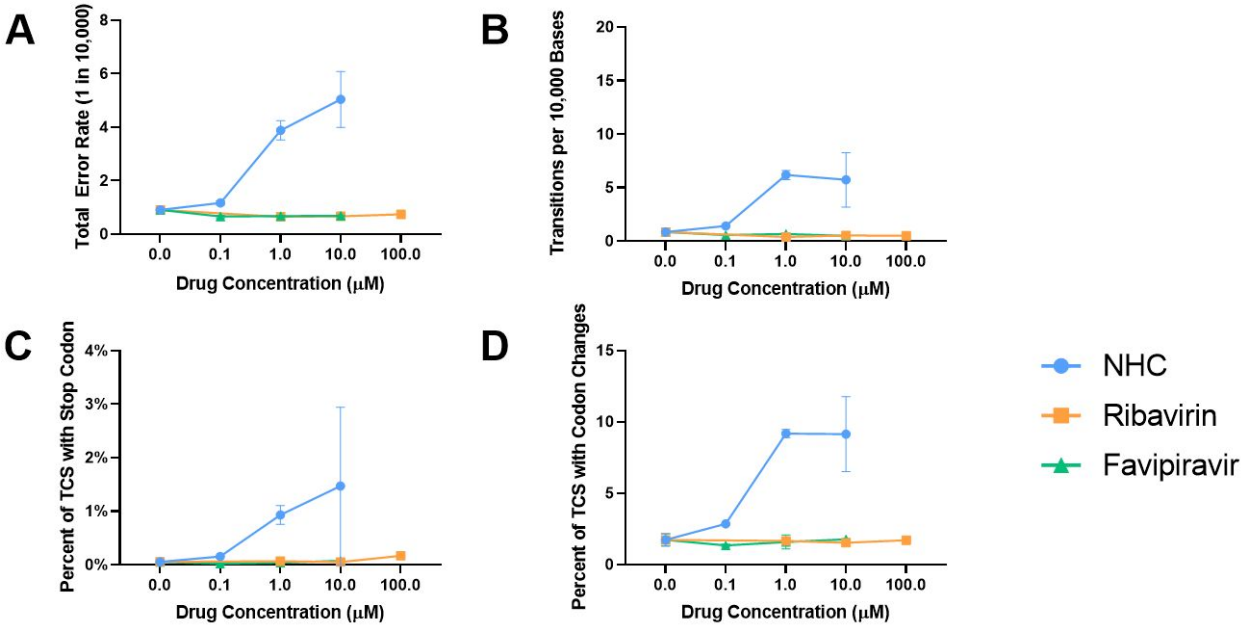

Panel A: Total error rate (error per 10,000) of NSP14 primer region of MERS-CoV under different compound and concentration conditions. Panel B: Cytidine to uracil (C to U) transition error rate (per 10,000) of NSP14 primer region of MERS-CoV in the drug panel. Panel C: Percent of template consensus sequences (TCS) with a change in codon to UAG, UAA, an UGA (stop codons) within the NSP14 primer region of MERS-CoV. Panel D: Percent of TCS with a change in codon (other than stop codons) within the NSP14 primer region of MERS-CoV. For all panels, the error bars indicate the range of each data set.

Supplemental Figure 4. Zika Virus NSP3 Primer Region Drug Panel Antiviral Activity and Mutagenic Effects

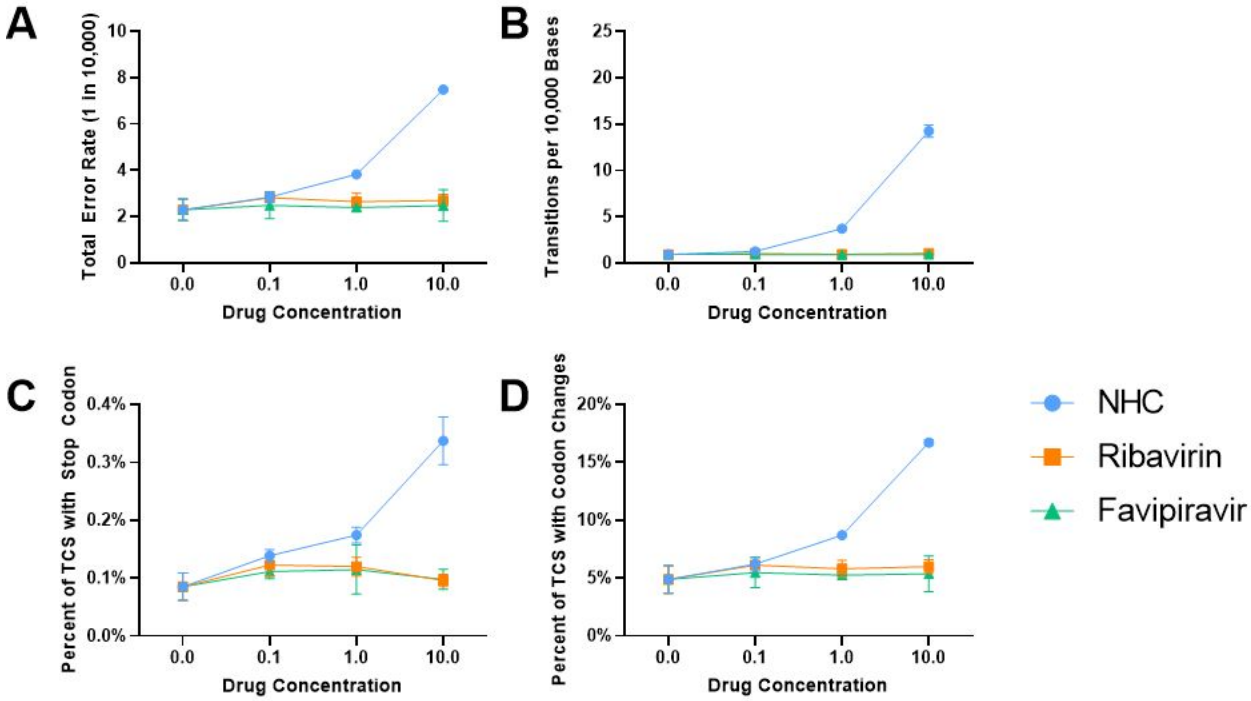

Panel A: Total error rate (error per 10,000) of NS3 primer region of Zika virus under different compound and concentration conditions. Panel B: Cytidine to uracil (C to U) transition error rate (per 10,000) of NS3 primer region of Zika virus in the drug panel. Panel C: Percent of template consensus sequences (TCS) with a change in codon to UAG, UAA, an UGA (stop codons) within the NS3 primer region of Zika virus. Panel D: Percent of TCS with a change in codon (other than stop codons) within the NS3 primer region of Zika virus. For all panels, the error bars indicate the range of each data set.